

# Construction and application of a liver cancer-targeting drug delivery system based on core-shell gold nanocages

Mengfei Ji,<sup>1,\*</sup> Xiaojing Qiu,<sup>2,\*</sup>  
Lin Hou,<sup>1</sup> Shengnan Huang,<sup>1</sup>  
Yuanmin Li,<sup>1</sup> Yang Liu,<sup>1</sup>  
Shaofeng Duan,<sup>3,4</sup> Yurong Hu<sup>1,5</sup>

<sup>1</sup>Henan Key Laboratory of Targeting Therapy and Diagnosis for Critical Diseases, School of Pharmaceutical Sciences, Zhengzhou University, Zhengzhou, People's Republic of China; <sup>2</sup>Henan Eye Institute, Henan Provincial People's Hospital, Zhengzhou, People's Republic of China; <sup>3</sup>College of Pharmacy, Henan University, Kaifeng, People's Republic of China; <sup>4</sup>Department of Orthopedics, The First Affiliated Hospital of Zhengzhou University, Zhengzhou, People's Republic of China; <sup>5</sup>Key Laboratory of Key Technology of Drug Preparation, Ministry of Education, Institute of Drug Discovery & Development, Zhengzhou University, Zhengzhou, People's Republic of China

\*These authors contributed equally to this work

**Background:** In order to achieve drug targeting and controlled release, we have successfully developed a novel drug release system DOX/AuNCs-PM-HA with gold nanocages (AuNCs) as photothermal cores, thermally responsive copolymer P(NIPAM-co-Am) (PM) as the near-infrared (NIR) stimuli gatekeeper and hyaluronic acid as a targeting ligand as well as a capping agent.

**Methods:** Cell uptake and cell viability were investigated. In vivo photoacoustic tomography imaging in H22 tumor bearing mice was analyzed for the tumor targeting effect of the nanocomplexes. Antitumor efficacy and the tissue distribution in vivo were investigated.

**Results:** In vitro results demonstrated that the DOX/AuNCs-PM-HA had significant anticancer activity against SMMC-7721 cells under NIR irradiation. Furthermore, in vivo photoacoustic tomography imaging of the nanocomplexes in H22 tumor bearing mice could indicate effective tumor targeting. Our studies on antitumor efficacy and the tissue distribution in vivo showed that many DOX/AuNCs-PM-HA nanocomplexes could efficiently accumulate at the tumor site so that they could inhibit the tumor growth effectively with limited side effects. The in vitro and in vivo results confirmed that the tumor-targeting and controlled-release drug system DOX/AuNCs-PM-HA with the combination of chemotherapy and photothermal therapy showed strong anti-tumor effect and would have great potential for future cancer therapy.

**Conclusion:** This tumor targeting DOX/AuNCs-PM-HA nanocomplex responded not only to the external stimuli of NIR, but also the internal stimuli of hyaluronidase, providing the potential for pinpointed and multi-stimuli responsive intracellular drug release.

**Keywords:** drug delivery, temperature-responsive polymers, hyaluronic acid, chemotherapy, photothermal therapy, photoacoustic imaging

## Introduction

Nanoscale carriers as controllable release systems in drug delivery have received much attention over the past few decades.<sup>1</sup> The controlled release system can release the loaded drug after being stimulated by external or internal stimuli.<sup>2</sup> Internal stimuli include pH and redox and high levels of certain enzymes,<sup>3,4</sup> while external stimuli include hyperthermia and magnetic field.<sup>5-8</sup> In some cases, the internal stimulus combined with the external stimulus will more effectively fine-tune their response to each stimulus and control the drug release more precisely.<sup>9</sup> However, it still remains a great challenge to develop an intelligent controlled-release system which can diagnose the tumor lesion site and realize precise control release at the tumor site.

Gold nanocages (AuNCs) are excellent nanoscale carriers due to their porous walls, hollow core and the property of localized surface plasmon resonance (LSPR) with

Correspondence: Yurong Hu  
Henan Key Laboratory of Targeting Therapy and Diagnosis for Critical Diseases, School of Pharmaceutical Sciences, Zhengzhou University, 100 Kexue Avenue, Zhengzhou 450001, People's Republic of China  
Tel +86 135 9804 0837  
Fax +86 371 6773 9546  
Email huyr@zzu.edu.cn

Shaofeng Duan  
College of Pharmacy, Henan University, Jin Ming Avenue, Kaifeng, 475004, People's Republic of China  
Tel +86 159 0378 9023  
Email sduan@henu.edu.cn

which the peaks are tunable in the near-infrared (NIR) region in light of the research previously reported.<sup>10</sup> Furthermore, many kinds of molecules and ligands can be readily modified on the surfaces of Au with Au–S bond.<sup>11,12</sup> The damaging effects of the anticancer drug doxorubicin (DOX) on DNA have recently been studied using a Raman electrochemical biosensor.<sup>13</sup> This type of a surface-enhanced Raman scattering sensor with plasmonic field modulation by drug-loaded gold nanoparticle carrier grid was then utilized for the development of targeted chemotherapeutic drug nanocarriers.<sup>14,15</sup> The thermosensitive and biodegradable properties of copolymer P(NIPAM-*co*-Am) (PM), *N*-isopropylacrylamide (NIPAM), have been reported.<sup>16</sup> In order to realize the drug control release, the thermosensitive PM could be used as the gatekeeper.<sup>17</sup> By copolymerization with acrylamide (Am), we could adjust the lower critical solution temperature (LCST) to an appropriate value. In this study, a copolymer PM with an appropriate LCST was prepared and employed as the gatekeeper to the gold nanocarrier. Hyaluronan (HA), a negatively charged natural polymer that is nontoxic and biodegradable,<sup>18–20</sup> can be degraded by the hyaluronidase (HAase) existing at both the internal and external regions of the tumor cells.<sup>21</sup> In addition, HA has the special affinity for CD44 receptors, which are overexpressed on cancer cells and can promote most of HA–nanoparticles to enter the cancer cells and enable degradation of the bound HA by the HAase in intracellular lysosomes.<sup>22–24</sup> Hence, as a tumor cell-specific targeted macromolecule, HA could also be used as a capping agent to control the drug release in response to HAase present in the intracellular environment.<sup>25–27</sup> As aforementioned, AuNCs, HA and the copolymer PM are appropriate materials to construct a novel drug delivery system.

Herein, we report a tumor-targeting, novel, multi-stimuli-responsive controlled drug release system, DOX/AuNCs-PM-HA, with AuNCs as the photothermal core, thermally responsive copolymer PM as the NIR-stimuli gatekeeper and HA as the targeting agent controlling the drug release in response to HAase (Scheme 1). Modification by conjugation of HA to the outer surface of the delivery vector rendered this delivery system targeting ability, leading to a higher drug concentration at the tumor site, reduced toxic and side effects of DOX and an improved curative effect. Meanwhile, modification with PM made the drug inside the delivery vector to be released only under NIR irradiation. Our drug-loaded nanocarriers responded to not only the external stimuli of NIR but also the internal stimuli of HAase, providing the potential for pinpointed and multi-stimuli-responsive intracellular drug release. Another potential possibility of our design is the synergistic effect of the combined photothermal therapy

(PTT) and chemotherapy (photothermal-chemotherapy). Moreover, the drug-loaded nanocarriers integrate the active targeting of HA and passive tumor targeting induced locally by the enhanced permeability and retention effect.<sup>28</sup> Furthermore, photoacoustic tomography (PAT) imaging of the DOX/AuNCs-PM-HA nanocomplexes can diagnose the tumor location, and the photothermal-chemotherapy also has been considered remarkably more efficient in cancer therapy (Scheme 1).

## Materials and methods

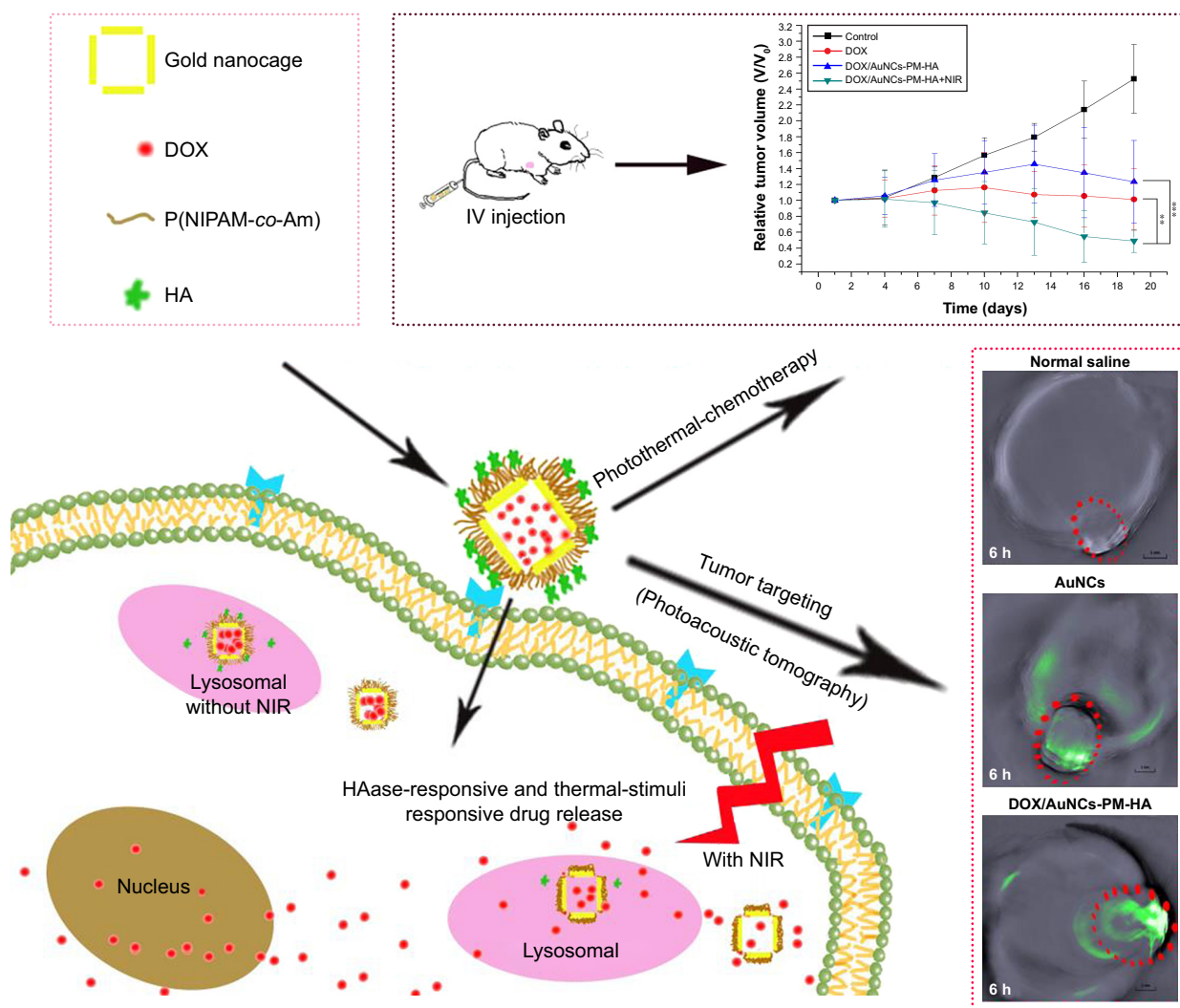
### Chemicals and materials

Tetrahydrofuran (THF) and 1,4-dioxane were obtained from Innovative Technology Inc. Ethylene glycol (99%) was purchased from Aladdin (Shanghai, People's Republic of China). 2-(Dodecylthiocarbonothioylthio)-2-methylpropionic acid *N*-hydroxysuccinimide ester (DIMA), 2,2'-azobis(isobutyronitrile) (AIBN; 95%) and Am (99%) were obtained from Aladdin and recrystallized from methanol before use. NIPAM (99%) was provided by Thermo Fisher Scientific (Shanghai, People's Republic of China) and recrystallized from hexane twice before use. 3-(4,5-Dimethylthiazol-2-yl)-2,5-diphenyltetrazolium bromide (MTT), poly(vinyl pyrrolidone) (PVP, molecular weight =55,000), chloroauric acid (HAuCl<sub>4</sub>·3H<sub>2</sub>O, 99.99%) and 4,6-diamidimino-2-phenylindole were all bought from Sigma-Aldrich (Boston, MA, USA). Sodium hyaluronate (HA, molecular weight =100 kDa) and HAase were provided by Sangon Biological Engineering Technology Co., Ltd (Shanghai, People's Republic of China). RPMI 1640 medium, streptomycin and penicillin were obtained from Thermo Fisher Scientific (Waltham, MA, USA). Fetal bovine serum was purchased from Biological Industries (Kibbutz Beit Haemek, Israel).

Deionized water (18.2 MΩ; EMD Millipore, Billerica, MA, USA) was utilized in all experiments.

### Synthesis of PM through reversible addition-fragmentation chain transfer (RAFT) polymerization

The copolymer P(NIPAM-*co*-Am) (PM) was synthesized via RAFT polymerization, which is a method reported previously.<sup>29</sup> In this study, the RAFT polymerization was conducted with AIBN as the initiator and DIMA as the chain transfer agent according to the references.<sup>28–30</sup> Briefly, NIPAM (1,146 mg, 10.125 mmol), 1,4-dioxane (5 mL), Am (80 mg, 1.125 mmol) and DIMA (11.5 mg, 0.025 mmol) were added to a 50 mL Schlenk flask under argon atmosphere. As soon as the mixture turned into a homogeneous solution



**Scheme 1** Schematic illustration for the preparation of the tumor-targeted, multi-stimuli responsive drug delivery system (DOX/AuNCs-PM-HA) as a combination of photoacoustic tomography and photothermal-chemotherapy.

**Note:** \*\* $p < 0.01$  and \*\*\* $p < 0.001$  represent significant difference between two groups.

**Abbreviations:** DOX, doxorubicin; AuNCs, gold nanocages; P(NIPAM-co-Am), copolymer of *N*-isopropylacrylamide and acrylamide; PM, copolymer of *N*-isopropylacrylamide and acrylamide; HA, hyaluronic acid; DOX/AuNCs-PM-HA, DOX-loaded, PM-grafted and HA-modified AuNCs; IV, intravenous; NIR, near-infrared irradiation; photothermal-chemotherapy, combination of photothermal therapy and chemotherapy.

after stirring for 10 min, AIBN (0.82 mg, 0.005 mmol) was added to it and was followed by magnetic stirring for 5 min. The reaction solution was then degassed by repeating three cycles of freeze–pump–thaw followed by heating gradually to 65°C, at which the reaction proceeded for about 4.5 h under stirring before it was stopped by dipping the flask into an ice–salt bath. Samples were withdrawn at the predetermined time intervals for analysis. Next, the content of the NIPAM monomer was measured by analyzing the collected samples with <sup>1</sup>H-nuclear magnetic resonance (<sup>1</sup>H-NMR) spectroscopy, and the highest percentage was found to be ~76%. The resulting copolymer was purified by slowly adding the reaction solution into cold diethyl ether to form a precipitate which was then dried under vacuum overnight leading to the desired trithiocarbonate

(TCA)-terminated polymer, PM-TCA, with a yield of 1.04 g (85%). <sup>1</sup>H-NMR (CDCl<sub>3</sub>, ppm): 1.02 (d, –CH<sub>2</sub>CH(CH<sub>3</sub>)<sub>2</sub>), 1.16 (s, –NHCH(CH<sub>3</sub>)<sub>2</sub>), 1.30–2.40 (m, polymer backbone protons), 4.03 (s, –NHCH), 4.22 (s, –C(=O)OCH<sub>2</sub>), 6.46 (bs, –C(=O)NH), where s is singlet proton, bs is broad singlet proton, d is doublet proton, and m is multiplet proton.

### Preparation of copolymer of NIPAM and acrylamide and sulfydryl (PM-SH)

The copolymer, PM-TCA, prepared through RAFT polymerization process, could be further modified in one step under mild conditions. The sulfhydrylation procedure of PM was carried out according to the literature reported previously.<sup>31,32</sup>

*N*-Butylamine (50 μL, 30-fold molar excess of thiocarbonylthio moiety) and a small amount of reducing agent, tris

(2-carboxyethyl) phosphine hydrochloride (catalytic amount), were added to the solution of PM-TCA (1.50 g, 0.075 mmol of thiocarbonylthio moieties) in THF (10 mL) followed by stirring at room temperature for 6 h under argon protection. Ultraviolet (UV)–Vis spectroscopy was used to monitor the reaction process. It was found that the yellow color of the reaction solution gradually faded away as time went on. Finally, addition of the THF solution into cold diethyl ether resulted in a precipitate, which was followed by drying under vacuum overnight leading to the target thiol-terminated PM-SH as a white powder with a yield of 1.38 g (92%).

## Synthesis of AuNCs

Ag nanocubes of 46 nm in diameter were synthesized as reported previously with a minor modification.<sup>33</sup> The AuNCs were prepared through the galvanic replacement reaction between HAuCl<sub>4</sub> and Ag nanocubes on the basis of a previously reported method.<sup>34,35</sup> In general, the HAuCl<sub>4</sub> solution was slowly dropped into the reaction mixture containing Ag nanocubes and PVP (1 mg/mL). UV–Vis spectroscopy was employed to monitor the formation of AuNCs with the major LSPR peak around 795 nm. Some more NaCl was added to the sample to convert Ag<sup>+</sup> into AgCl, and then the resulting mixture was centrifuged and washed with water several times to remove PVP, AgCl and NaCl. Finally, the AuNCs were dispersed in deionized water for the next step.

## Preparation of AuNCs-PM

PM-SH (425 mg) was suspended in 10 mL of deionized water and whirled until it was completely dissolved. Five milliliters of AuNC solution (8 pM) was dropped quickly into the solution of PM-SH and stirred at room temperature with argon protection in the dark for 72 h. The unreacted polymer in the solution was then removed through centrifuging at a speed of 8,000 rpm for 20 min. After that, the solution of AuNCs-PM was washed for three times with 3 mL of deionized water and then redispersed in 1.0 mL water for the next step.

## Preparation of DOX/AuNCs-PM-HA

DOX was added to the AuNCs-PM solution prepared earlier, which was followed by stirring at 42°C in the dark for 6 h. After that, the solution was cooled in an ice bath for 0.5 h, followed by centrifuging and repeated washing with deionized water. All the washing solutions were collected. One hundred microliters of HA (1 mg/mL) was dropped into the mixed solution, followed by shaking at 25°C for about 30 min. The resulting mixture was then centrifuged at a speed of 6,500 rpm for 15 min and washed several times

with deionized water. Next, the mixture was resuspended in 1.5 mL water and denoted as DOX/AuNCs-PM-HA. UV–Vis spectrophotometer was utilized to determine the concentration of DOX in the supernatant and measure the drug loading efficiency. The loading capacity of DOX/AuNCs-PM-HA was estimated as the weight percentage of DOX drug on DOX/AuNCs-PM-HA nanocarriers.

The calculation formulas of the entrapment efficiency and drug loading degree are as follows: entrapment efficiency = (weight of DOX in DOX/AuNCs-PM-HA)/(initial weight of DOX); loading content = (weight of DOX in DOX/AuNCs-PM-HA)/(weight of DOX/AuNCs-PM-HA).<sup>36</sup> Our experimental results showed that the DOX encapsulation efficiency was 83.2% and the loading degree reached up to 4.2%.

## Multi-stimuli-responsive release experiments

In order to detect the capacity of HAase and NIR to trigger the release of DOX from DOX/AuNCs-PM-HA under different environments, we dispersed the DOX/AuNCs-PM-HA in PBS buffer (pH 7.4) and acetate buffer (pH 4.5) containing or exclusive of HAase (150 U/mL) at 37°C. Specimens (50 µL) were collected from the mixture solution every 1 h and replenished with an equal volume of the buffer solution. Subsequently, the specimens were centrifuged and analyzed, followed by measuring of the concentration of the released DOX by UV–Vis spectroscopy at 480 nm on the basis of standard curve (Figure S1).

## Cell culture

The human hepatocarcinoma SMMC-7721 cell line was provided by the Institute of Biochemistry and Cell Biology, CAS (Shanghai, People's Republic of China). SMMC-7721 cells were incubated in RPMI 1640 supplemented with streptomycin (100 µg/mL), penicillin (100 U/mL) and 10% fetal bovine serum at 37°C in an incubator containing 5% CO<sub>2</sub>.

## Cellular uptake

After the SMMC-7721 cells had been cultured in a six-well plate at 2.5×10<sup>5</sup> cells/well for 24 h, the old medium was discarded. Then, 2 mL of fresh culture medium containing DOX/AuNCs-PM-HA (AuNC content at 40 µg/mL) was added to incubate the cells for 3 h. Next, the culture medium was substituted by fresh medium and the cells were subjected to NIR laser (808 nm, 1.5 W/cm<sup>2</sup>, 7 min). Then, SMMC-7721 cells were continued to be cultured for 1 h. Finally, the culture medium was substituted by 4,6-diamidino-2-phenylindole in fresh cell medium. After incubation for 15 min, the old medium was discarded and the cells were rinsed three times with PBS.

## In vitro cytotoxicity assays

The SMMC-7721 cells were plated in sextuplicate at a density of 5,000 cells/well in 96-well assay plates. After incubation under a humidified environment of 5% CO<sub>2</sub> at 37°C for 12 h, the cells were exposed to DOX (0, 0.42, 0.84, 1.26 and 1.68 µg/mL), DOX/AuNCs-PM-HA (containing 0, 0.42, 0.84, 1.26 and 1.68 µg/mL of DOX) or AuNCs-PM-HA alone (AuNC content at 0, 10, 20, 30 and 40 µg/mL). After incubation for 24 h, the cell viability was detected by MTT assay.

## In vivo tissue distribution of DOX/AuNCs-PM-HA

Female Kunming mice (20–22 g) were purchased from the experimental animal center of Henan Province. All experiments complied with the National Laboratory Animal Management Regulations (People's Republic of China 1988) and Guidance on the Treatment of Experimental Animals (People's Republic of China; 2006) and were conducted under a license with local ethical approval by the Life Science Ethics Committee Review Board of Zhengzhou University. The tumors were formed by subcutaneous injection of H22 tumor cells into the right axilla of each female mouse. When the size of the tumors reached ~200 mm<sup>3</sup>, the mice were randomized into three groups (n=3 per group). Normal saline (NC; control), DOX solution or DOX/AuNCs-PM-HA were injected via the tail vein at a dose of 2 mg DOX/kg. The mice of DOX/AuNCs-PM-HA group were irradiated by 808 nm NIR laser (1.5 W/cm<sup>2</sup>, 7 min). At 0.5, 6 and 12 h after injection, the mice were sacrificed and the hearts, lungs, spleens, livers, kidneys and tumors were collected. All the organs were sectioned at 5 µm by freezing microtome section. The DOX imaging of the frozen sections was obtained using a fluorescence microscope (Nikon Eclipse 50i; Nikon Corporation, Tokyo, Japan).

## In vivo PAT imaging of the DOX/AuNCs-PM-HA in H22 tumor-bearing mice

When the volume of tumors grew up to 200 mm<sup>3</sup>, the mice were used for the PAT imaging using an in vivo multispectral optoacoustic tomography imaging system (in Vision 128; iThera medical GmbH, Munich, Germany). The skin of Kunming mice was exposed by depilation and fully anesthetized with 2% isoflurane (RWD Life Science, Shenzhen, People's Republic of China) in oxygen at a flow rate of 1 L/min. The body was then covered with TM-100 ultrasonic coupling gel. A thin polyethylene membrane was utilized as an animal holder to protect the mouse from being immersed in water and allow acoustic coupling between the mouse and the transducer array.<sup>37,38</sup> H22 tumor-bearing mice were injected

with AuNCs and DOX/AuNCs-PM-HA (AuNC content at 23.78 mg/kg) via tail vein. PAT imaging of the H22-bearing mice was obtained at preestablished time points (0, 3, 6 and 12 h postinjection) at a wavelength of 800 nm.

## Tumor suppression study

After the tumors had developed to about 100 mm<sup>3</sup>, the mice were randomly divided into four groups (n=5 per group) as follows: 1) NC (control), 2) DOX solution, 3) DOX/AuNCs-PM-HA and 4) DOX/AuNCs-PM-HA+NIR (808 nm, 1.5 W/cm<sup>2</sup>, 7 min). All the aforementioned solutions were injected via the tail vein at a frequency of once every 3 days for a total of five times. The dose of DOX for each mouse was 2 mg/kg and the dose of AuNCs was 47.62 mg/kg. After treatment, the tumor volume and the body weight of the mice were measured every 3 days. The tumor volume was calculated as (tumor width)<sup>2</sup> × (tumor length)/2.<sup>38</sup>

## Histologic analyses

After treating for five times with the therapies, the mice were sacrificed. The tumors and major organs (livers, hearts, lungs, spleens and kidneys) were collected and immersed into 4% paraformaldehyde for 24 h. Afterward, they were encapsulated in paraffin and sectioned for histologic analysis by hematoxylin and eosin (H&E) staining.<sup>39,40</sup>

## Statistical analysis

All the experiments were carried out at least three times. All data were presented as mean ± SD. Statistical comparisons were evaluated with Student's *t*-test. *P*<0.05 was considered to be statistically significant.

## Results and discussion

### Synthesis and characterization of PM and PM-SH

PM is one of the most intensive investigated thermoresponsive polymers. When the temperature increases above 39°C, the polymer could sustain an invertible phase transition in water solution from a stretch hydrophilic chain into an agglomerative hydrophobic spherule (Figure 1A). TCA-modified and temperature-sensitive copolymer PM (P(NIPAM-*co*-Am)-TCA) was synthesized using NIPAM and Am as the monomers, DIMA as the chain transfer agent and AIBN as the initiator by the RAFT method (Figure S1). As seen in Figure 1B, the LCST of PM was about 39°C, which is above the body temperature (37°C) but below the heated temperature (42°C). Samples were collected at different time intervals and analyzed through <sup>1</sup>H-NMR spectroscopy to investigate the conversion of the monomer

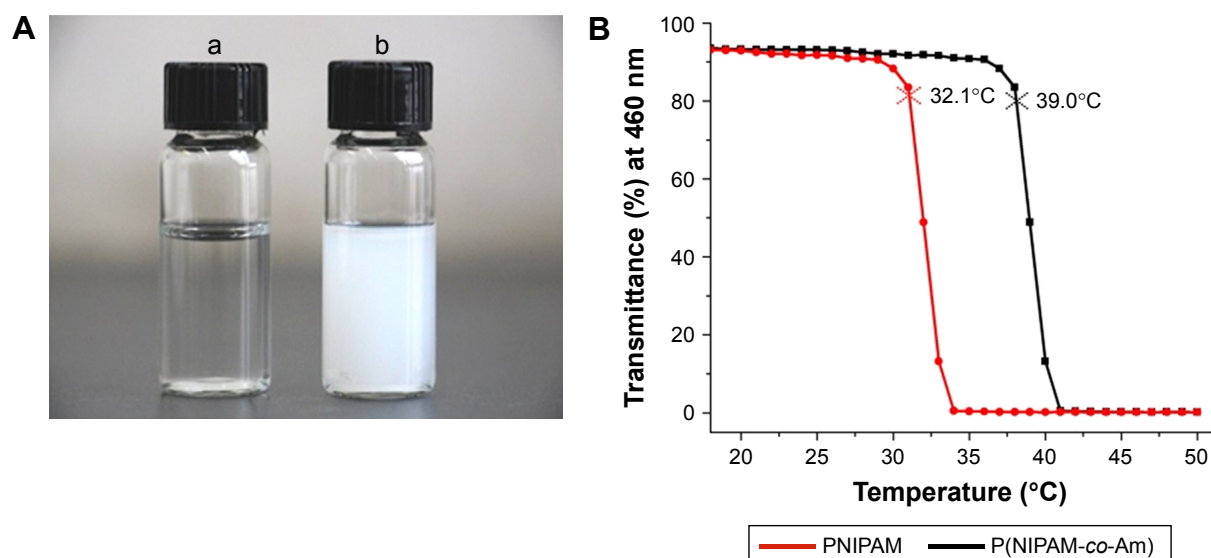


**Figure 1** The temperature sensitivity of PNIPAM and PM.

**Notes:** (A) Different solution states of P(NIPAM-co-Am) at room temperature (a) and 42°C (b). (B) The LCST detected spectrophotometrically with the solution being heated at a speed of 1°C/min. The temperature of the initial polymer solution with 90% of initial transmittance (at 460 nm) was defined as the LCST. The red curve is the transmittance curve of PNIPAM and the black curve is the transmittance curve of PM.

**Abbreviations:** Am, acrylamide; LCST, lower critical solution temperature; PM, copolymer of *N*-isopropylacrylamide and acrylamide; PNIPAM, poly(*N*-isopropylacrylamide).

NIPAM (conversion finally reached ~76%) and determine the chemical structure of poly(NIPAAm-co-AAm) copolymers as well (Figure S2). At the same time, equivalents of the reaction mixture were taken and analyzed by gel permeation chromatography to obtain the molecular weight of the polymer samples. The linear increase in the number-average molecular weight ( $M_n$ ) with conversion was used to study how the chain transfer agent DIMA affected the polymerization of NIPAM. The  $M_n$  had a linear increase from 9,000 to 23,400 g/mol (Figure S3B). A kinetic plot of the polymerization (Figure S3A) showed a linear pseudo-first-order regime up to a monomer conversion of 76%, which also indicated an induction period of 24 min.

Due to the existence of reducing agent tris(2-carboxyethyl) phosphine hydrochloride limiting the formation of disulfide in the aminolysis process, the terminal TCA groups of the chain transfer agent were converted to thiols through aminolysis. As soon as butylamine was added, PM-SH was generated (Figure S1) and the yellow color of the P(NIPAM-co-Am)-TCA polymer solution immediately disappeared. With the decrease in absorbance at 310 nm, consumption of TCA groups could be verified by UV-Vis spectroscopy (Figure S4).

## Synthesis and characterization of AuNCs-PM

Ag nanocubes with the LSPR peak at 437 nm (Figure S5A) were synthesized and well characterized by transmission electron microscopy (TEM; Figure S5B). The AuNCs were

prepared using Ag nanocubes as the sacrifice templates through the galvanic replacement reaction. The LSPR peak of AuNCs was at 795 nm (Figure S5C), which fitted to the laser excitation wavelength of the NIR laser source. Figure S5D shows the typical TEM images of AuNCs with the pore diameter of 5–8 nm and an edge length of 46 nm. Furthermore, the narrow absorption spectra in Figure S5A and S5C demonstrate that the Ag nanocubes and AuNCs showed good uniformity and dispersity in water.

To realize our design, we covalently conjugated PM-SH to the surface of the AuNCs via the formation of thiolate–Au bond. TEM images of AuNCs-PM are shown in Figure 2A. The LSPR peak of AuNCs-PM shifted from 795 to 807 nm compared to the AuNCs, suggesting the successful synthesis of AuNCs-PM (Figure 2B). The hydrodynamic diameter and the zeta potential of AuNCs and AuNCs-PM were measured using dynamic light scattering. We could observe the oscillation of the mean hydrodynamic diameter of AuNCs-PM stimulated by the ever-changing temperature: the particle size shrank on heating to 42°C and recovered to its initial state under 37°C. As shown in Figure 2C, the hydrodynamic diameters of AuNCs-PM increased about 20 and 7 nm compared with those of AuNCs at 37°C and 42°C, respectively.

Some methods were used to verify whether PM-SH was successfully grafted onto the surface of AuNCs. For instance, the obvious coating morphology in the TEM images (Figure 2A) demonstrated uniform distribution of the copolymer on the surface of AuNCs. The LSPR peak of AuNCs-PM

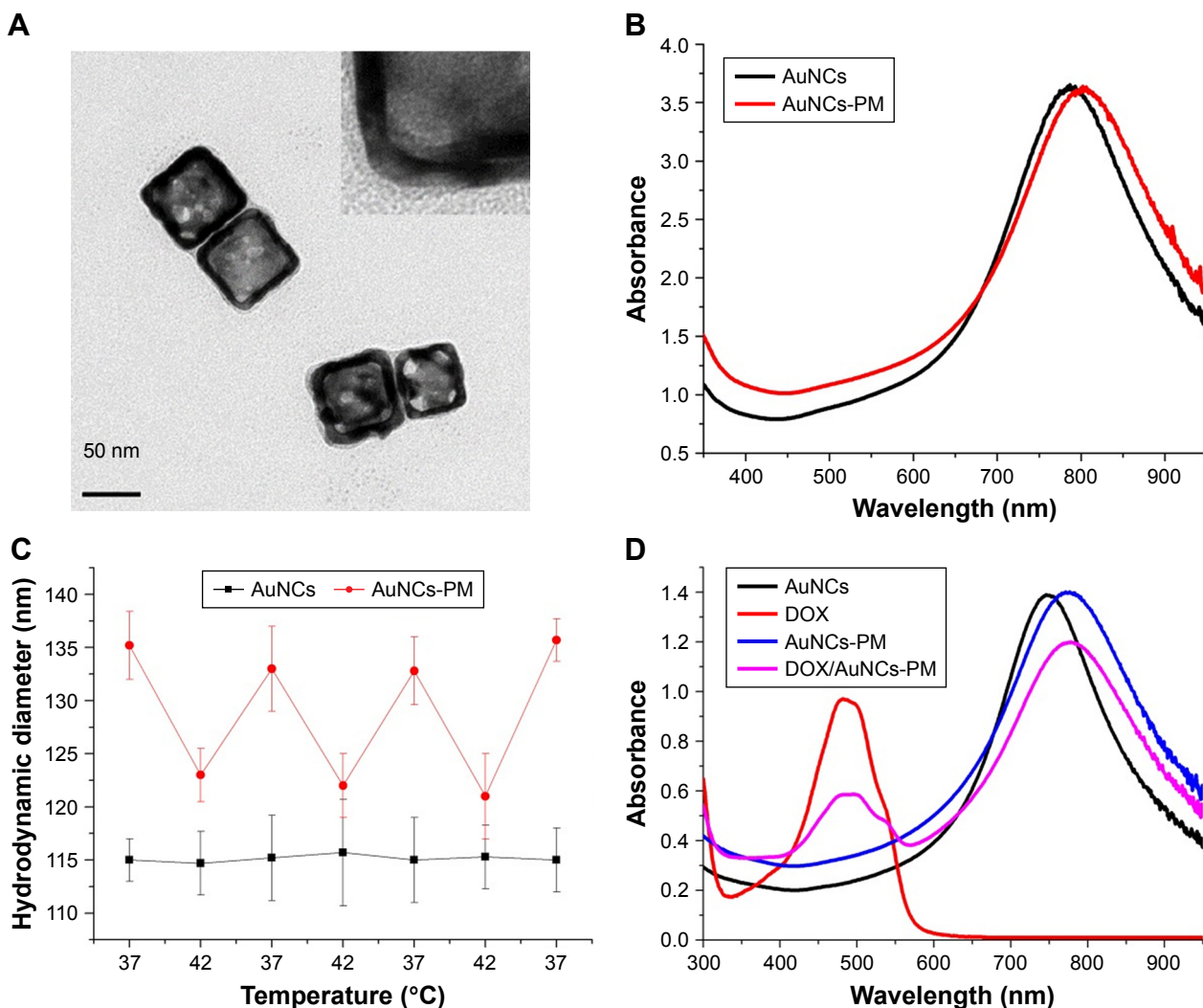


**Figure 2** Characterization of AuNCs-PM and DOX/AuNCs-PM.

**Notes:** (A) TEM images of the AuNCs-PM. A magnified TEM picture of the AuNCs-PM is shown in the inset. (B) UV-Vis absorption spectra of AuNCs and AuNCs-PM. (C) Mean hydrodynamic diameters of AuNCs and AuNCs-PM plotted as a solution temperature function. (D) UV-Vis absorption spectra of AuNCs, DOX solution, AuNCs-PM and DOX/AuNCs-PM.

**Abbreviations:** AuNCs, gold nanocages; AuNCs-PM, PM-grafted AuNCs; DOX, doxorubicin; DOX/AuNCs-PM, DOX-loaded and PM-grafted AuNCs; DOX/AuNCs-PM-HA, DOX-loaded, PM-grafted and HA-modified AuNCs; HA, hyaluronic acid; PM, copolymer of *N*-isopropylacrylamide and acrylamide; TEM, transmission electron microscopy; UV-Vis, ultraviolet-visible.

and DOX/AuNCs-PM, shown in Figure 2D, demonstrates that DOX was successfully loaded into the AuNCs-PM nanocomplexes. Average hydrodynamic diameter of the DOX/AuNCs-PM-HA was  $141 \pm 4.2$  nm after modification with HA (Figure 3A). The zeta potential of AuNCs was about  $-14.3 \pm 2.7$  mV, while that of AuNCs-PM increased dramatically to  $5.3 \pm 1.4$  mV (Figure 3B). As for the DOX/AuNCs-PM-HA nanocomplexes, the zeta potential changed from  $7.2 \pm 2.6$  mV of DOX/AuNCs-PM to  $-1.1 \pm 1.6$  mV.

## Drug loading

To load the drug into AuNCs, the AuNCs were suspended in the DOX aqueous solution (0.2 mM) and then agitated at  $42^\circ\text{C}$  for 12 h, which was followed by cooling in an ice bath

to realize the entire sealing of the holes of AuNCs by the shape changing of the polymer PM on the DOX/AuNCs-PM nanocomplexes. Drug loading efficiency of DOX/AuNCs-PM-HA was 4.2%. The DOX/AuNCs-PM nanocomplexes were then wrapped by HA through electrostatic adsorption due to their negative charge (Figure 3A and B).

## Multi-stimuli-responsive release

Previous studies have indicated that the tunable LSPR peaks of AuNCs are in the NIR region. Therefore, AuNCs can be used as photothermal agents.<sup>40,41</sup> To evaluate the potential of the AuNCs-PM-HA for PTT, the AuNCs-PM-HA solution (AuNCs content at  $40 \mu\text{g/mL}$ ) was exposed to NIR laser (808 nm,  $1.5 \text{ W/cm}^2$ , 10 min). The results show that the temperature

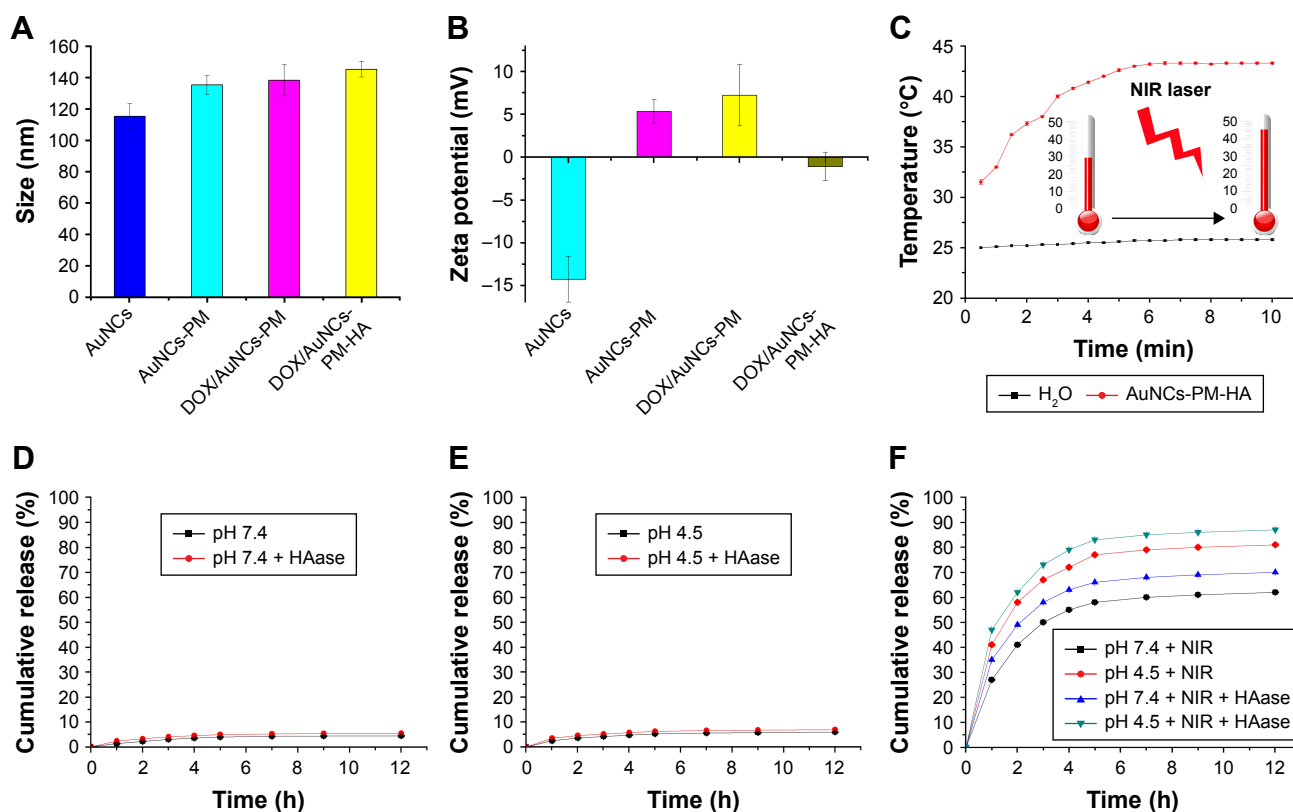


**Figure 3** Characterization, photothermal conversion and the release profile of functionalized AuNCs.

**Notes:** (A) Sizes of AuNCs, AuNCs-PM, DOX/AuNCs-PM and DOX/AuNCs-PM-HA. (B) Zeta potentials of AuNCs, AuNCs-PM, DOX/AuNCs-PM and DOX/AuNCs-PM-HA. (C) Photothermal curves of the AuNCs-PM-HA (AuNCs content at 40  $\mu\text{g}/\text{mL}$ ) and  $\text{H}_2\text{O}$  irradiated by NIR laser (808 nm, 1.5  $\text{W}/\text{cm}^2$ ). (D and E) DOX release curves of DOX/AuNCs-PM-HA at pH 7.4 and pH 4.5, with or without HAase. (F) DOX release curves of DOX/AuNCs-PM-HA at pH 7.4 and pH 4.5 with NIR laser irradiation (808 nm, 1.5  $\text{W}/\text{cm}^2$ , 7 min), with or without HAase.

**Abbreviations:** AuNCs, gold nanocages; AuNCs-PM, PM-grafted AuNCs; DOX, doxorubicin; DOX/AuNCs-PM, DOX-loaded and PM-grafted AuNCs; DOX/AuNCs-PM-HA, DOX-loaded, PM-grafted and HA-modified AuNCs; HA, hyaluronic acid; HAase, hyaluronidase; NIR, near-infrared irradiation; PM, copolymer of *N*-isopropylacrylamide and acrylamide.

of AuNCs-PM-HA solution rose significantly within 5 min and then was maintained stably at 42°C (Figure 3C).

To further confirm that NIR and intracellular HAase played an important role in the controlled release of drug, we conducted a series of experiments with different incubation time periods under various environments. As shown in Figure 3D, the DOX/AuNCs-PM-HA could release only trace amount of DOX in PBS buffer (pH 7.4) within 12 h. In addition, no remarkable augment was detected in the presence of HAase. Besides, at pH 4.5, similar drug release behavior of DOX/AuNCs-PM-HA nanocomplexes was observed (Figure 3E). According to the above results, the DOX/AuNCs-PM-HA nanocomplexes would retain wonderful encapsulating efficiency and stability in mimetic physiological conditions (pH 7.4) and intercellular lysosomes (pH 4.5) without NIR.

Next, we investigated the drug release of DOX/AuNCs-PM-HA with NIR (1.5  $\text{W}/\text{cm}^2$ , 808 nm, 7 min) at pH 7.4 and 4.5 and with or without HAase. An arresting and burst

release of DOX was detected compared to the above results. When the temperature was raised above 39°C, the LCST of the PM, the stretch state of PM changed to frizzy conformation. After that, the holes on the nanocages were exposed and the release of DOX was significantly enhanced. HAase could degrade the HA on the outer layer. When NIR and HAase existed simultaneously, the release of DOX was the most significant (Figure 3F).

Based on the above experimental results, we found that DOX could not be released adequately without NIR, appropriate pH or HAase. So, DOX/AuNCs-PM-HA was able to prevent premature leakage of the drug and accurately release the drug in the cancer cells.

## Cell uptake

Based on the success in controlling the release of DOX/AuNCs-PM-HA, we further investigated its cellular uptake and intracellular release activity in liver cancer cells using fluorescence microscopy images. SMMC-7721 cells were

cultivated with the DOX/AuNCs-PM-HA and DOX/AuNCs-PM nanocomplexes for 4 h, and then washed thrice with PBS to discard the extracellular nanocomplexes and incubated with fresh medium. We could hardly see the red fluorescence of DOX (Figure 4A and B) after 1 h. However, after exposure to NIR (808 nm, 1.5 W/cm<sup>2</sup>, 7 min), an obvious enhanced red fluorescence was found in the nuclei of DOX/AuNCs-PM-HA+NIR group (Figure 4C). It was easily observed that NIR laser radiation could trigger the release of DOX in DOX/AuNCs-PM-HA nanocomplexes.

### Cell viability

The viability of SMMC-7721 cells was measured by MTT assay. Figure 5A indicates that the cell viability of SMMC-7721 treated with AuNCs-PM-HA at different concentrations (AuNCs content at 0–40 µg/mL) was higher than 95%. It should be mentioned that AuNCs-PM-HA+NIR (AuNCs content at 40 µg/mL, 808 nm, 1.5 W/cm<sup>2</sup>, 7 min)

could decrease the viability of SMMC-7721 cells to 78.6%. SMMC-7721 cells were cultured with DOX/AuNCs-PM-HA with or without NIR, DOX (DOX content at 0, 0.42, 0.84, 1.26 and 1.68 µg/mL) and AuNCs-PM-HA with NIR irradiation (808 nm, 1.5 W/cm<sup>2</sup>, 7 min) for 24 h, respectively. As shown in Figure 5B, the cell viability of DOX/AuNCs-PM-HA+NIR (DOX content at 1.68 µg/mL) group (photothermal-chemotherapy) was significantly decreased to 39.25%. It could be easily noticed that the antitumor effect of chemo-photothermal therapy was obviously better than any one of the chemotherapies or PTT alone, generating a commendable synergistic effect (Figure 5B).

### In vivo tissue distribution of the DOX/AuNCs-PM-HA

To investigate the distribution of DOX in vivo, the DOX fluorescence images of the frozen section of the major organs at different time points were recorded (Figure 6). It was found that free DOX was mainly distributed in the liver, lung and

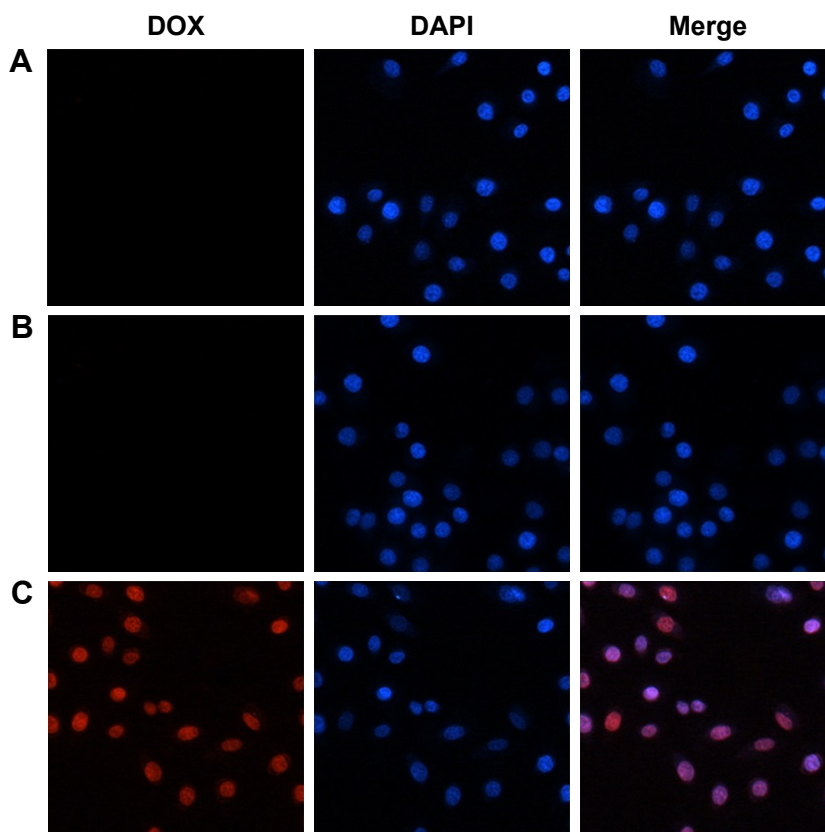


**Figure 4** Cellular uptake of SMMC-7721 cells. SMMC-7721 cells stained by DAPI and cultured with DOX/AuNCs-PM and DOX/AuNCs-PM-HA (DOX and AuNCs content at 1.68 and 40 µg/mL, respectively) for 4 h at 37°C; magnification  $\times 400$ .

**Notes:** (A) DOX/AuNCs-PM, (B) DOX/AuNCs-PM-HA, (C) DOX/AuNCs-PM-HA+NIR (808 nm, 1.5 W/cm<sup>2</sup>, 7 min). Blue fluorescence: nuclei stained by DAPI, red fluorescence: DOX in cells.

**Abbreviations:** AuNCs, gold nanocages; DAPI, 4,6-diamidimo-2-phenylindole; DOX, doxorubicin; DOX/AuNCs-PM, DOX-loaded and PM-grafted AuNCs; DOX/AuNCs-PM-HA, DOX-loaded, PM-grafted and HA-modified AuNCs; DOX/AuNCs-PM-HA+NIR, DOX/AuNCs-PM-HA with NIR laser; HA, hyaluronic acid; NIR, near-infrared irradiation; PM, copolymer of *N*-isopropylacrylamide and acrylamide.

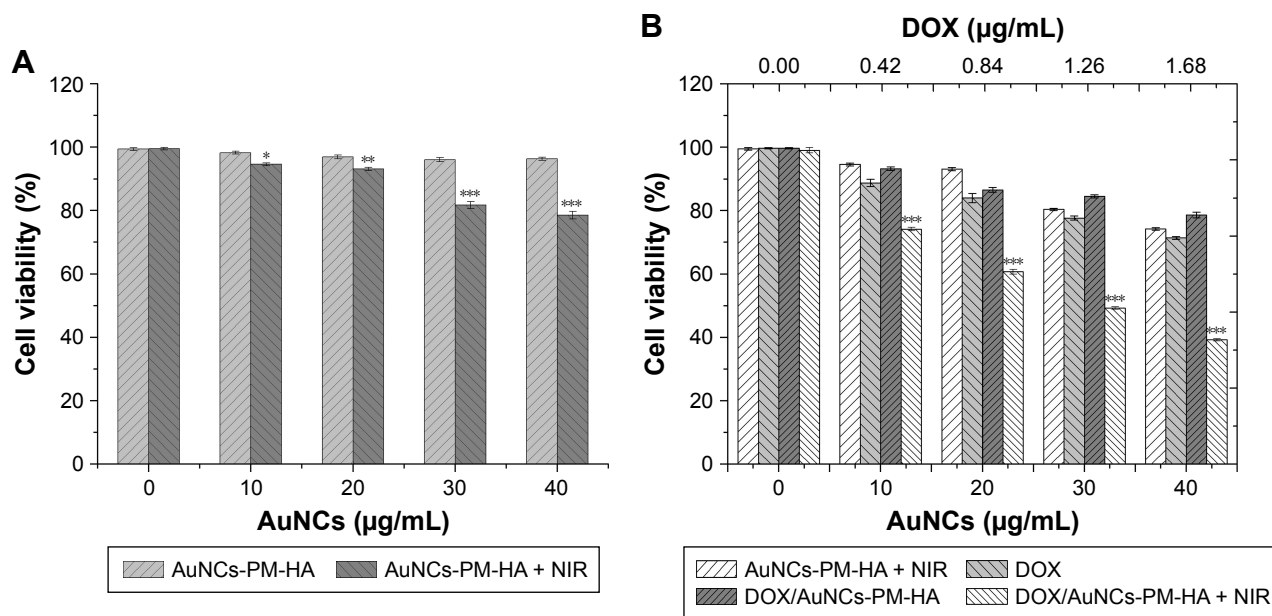


**Figure 5** Cell viability of SMMC-7721 cells.

**Notes:** (A) Cell viability of SMMC-7721 cells incubated for 24 h with different concentrations of AuNCs-PM-HA with or without NIR irradiation (808 nm, 1.5 W/cm<sup>2</sup>, 7 min). (B) Viability of SMMC-7721 cells incubated for 24 h with DOX/AuNCs-PM-HA with or without NIR, free DOX (DOX content at 0, 0.42, 0.84, 1.26, 1.68 µg/mL) and AuNCs-PM-HA with NIR irradiation (808 nm, 1.5 W/cm<sup>2</sup>, 7 min). \**p*<0.05, \*\**p*<0.01, and \*\*\**p*<0.001 indicate significant difference between two groups.

**Abbreviations:** AuNCs, gold nanocages; DOX, doxorubicin; DOX/AuNCs-PM-HA, DOX-loaded, PM-grafted and HA-modified AuNCs; HA, hyaluronic acid; NIR, near-infrared irradiation; PM, copolymer of *N*-isopropylacrylamide and acrylamide.

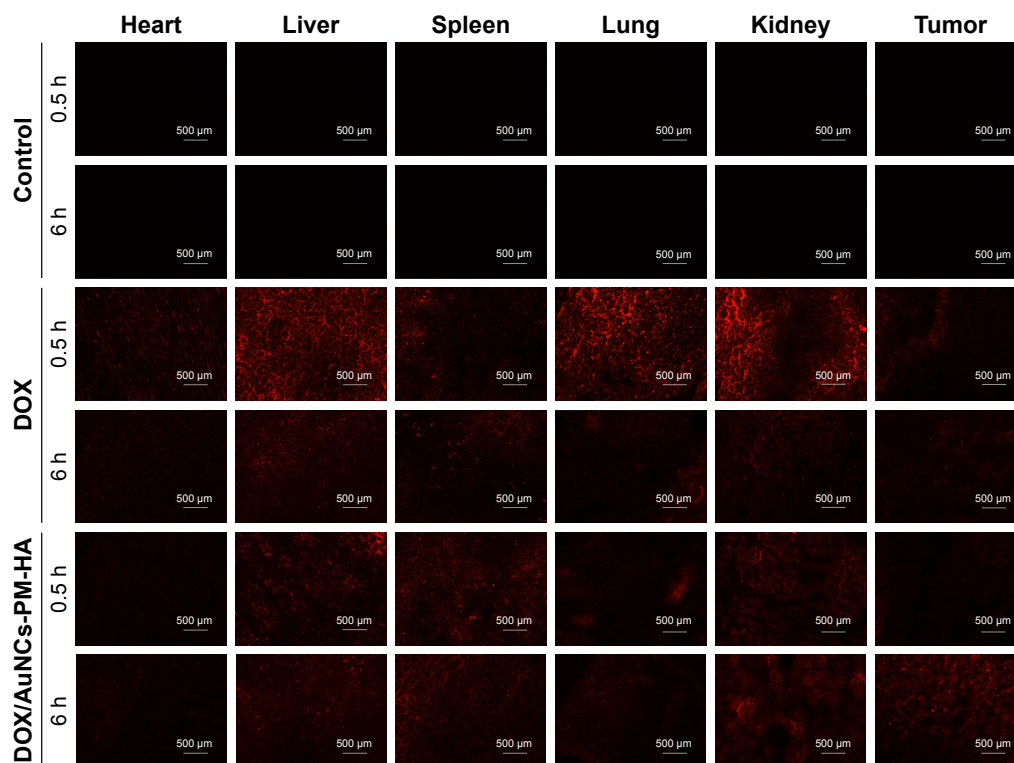


**Figure 6** Fluorescence microscopy images of DOX in slices of tumors and other organs after injection (0.5 and 6 h) with normal saline (control), DOX solution (free DOX), DOX/AuNCs-PM-HA (200×).

**Notes:** The scale bars represent 500 µm. The red fluorescence is expressed by released DOX. The tumors of DOX/AuNCs-PM-HA group were illuminated by NIR laser (1.5 W/cm<sup>2</sup>, 808 nm, 7 min) at 0.5 and 6 h postinjection, respectively.

**Abbreviations:** AuNCs, gold nanocages; DOX, doxorubicin; DOX/AuNCs-PM-HA, DOX-loaded, PM-grafted and HA-modified AuNCs; HA, hyaluronic acid; NIR, near-infrared irradiation; PM, copolymer of *N*-isopropylacrylamide and acrylamide.

kidney after treatment. The red fluorescence intensity of tumor was very weak and decreased with time since free DOX was eliminated from the tissue very quickly. Compared with the free DOX and NC groups, the DOX/AuNCs-PM-HA group had more distribution of DOX in the tumor. Especially, the NIR laser could stimulate the release of DOX in 6 h. Because of the enhanced permeability and retention effect in tumor tissues and the irradiation of 808 nm NIR laser, the DOX/AuNCs-PM-HA nanocomplexes could accumulate highly in the tumor site and control the release of DOX by NIR. We could hardly see the red fluorescence of DOX in the heart of DOX/AuNCs-PM-HA group. It demonstrates that the DOX/AuNCs-PM-HA nanocomplexes might have smaller cardiotoxicity than free DOX.<sup>42</sup>

### In vivo PAT imaging

In order to examine the PAT capability of AuNCs and DOX/AuNCs-PM-HA and the tumor-targeting potency of DOX/AuNCs-PM-HA in vivo, the H22 tumor-bearing mice were scanned by PAT imaging. Images obtained at 0, 3, 6 and 12 h after intravenous injection with NC, AuNCs and DOX/AuNCs-PM-HA (AuNCs content at 23.78 mg/kg) are shown in Figure 7. Signal enhancement at the tumor site is marked by a red dotted line. It was obvious that the signal intensity of tumor sites after treatment was much higher than that

before treatment. After treatment, the DOX/AuNCs-PM-HA accumulated more in the tumor site than AuNCs due to the targeting ability of HA. In addition, no photoacoustic signal was observed for the NC group. Compared with the AuNCs group, the photoacoustic signal intensity of the DOX/AuNCs-PM-HA group at the tumor site at 12 h postinjection was also very strong. Notably, the PAT signals showed maximum accumulation at the tumor site at 6 h postinjection for the AuNCs and the DOX/AuNCs-PM-HA. Furthermore, the PAT imaging results could also be used to screen the experimental conditions, which led to the conclusion that 6 h postinjection was the optimum timing for PTT in vivo for the DOX/AuNCs-PM-HA nanocomplex-mediated NIR irradiation.

### In vivo antitumor efficacy and toxicity assays

To further investigate the antitumor efficacy of the targeted delivery system DOX/AuNCs-PM-HA in vivo, H22 tumor-bearing mice were treated with 1) NC (control), 2) DOX solution, 3) DOX/AuNCs-PM-HA and 4) DOX/AuNCs-PM-HA+NIR via tail vein injection once in every 3 days for a total of five times. The tumors of DOX/AuNCs-PM-HA+NIR group were irradiated for 7 min by 808 nm NIR laser ( $1.5 \text{ W/cm}^2$ ) at 6 h posttreatment. The body weight changes

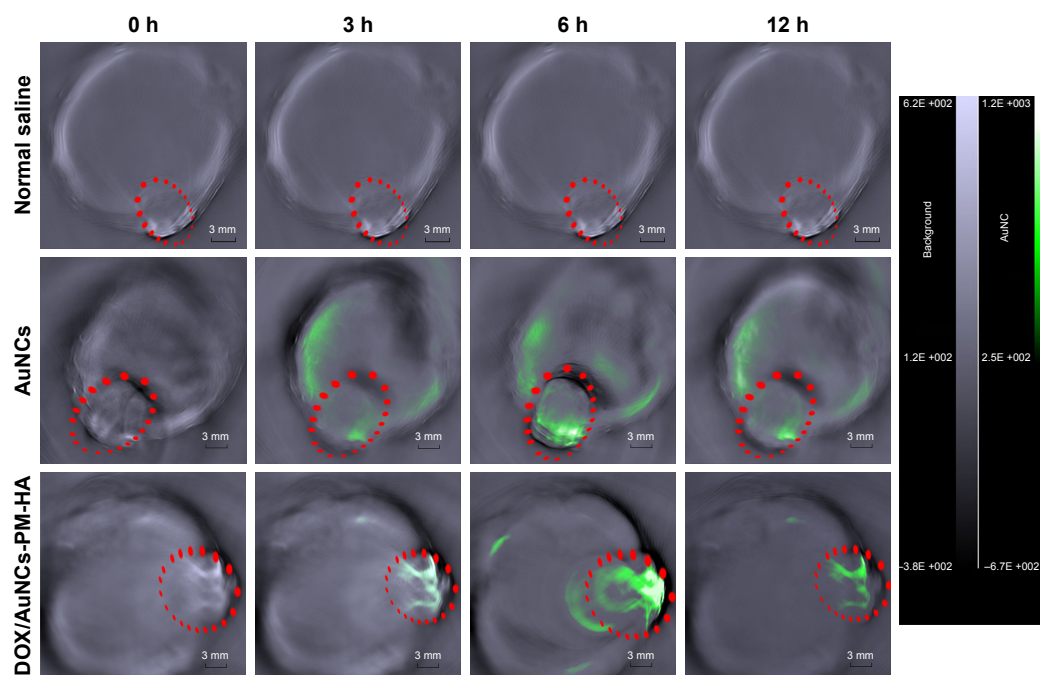


**Figure 7** In vivo photoacoustic tomography image of H22 tumor (marked as green)-bearing mice treated with normal saline, AuNCs, DOX/AuNCs-PM-HA (AuNCs content at 23.78 mg/kg).

**Note:** The scale bars represent 3 mm. The tumor areas are marked by red ellipses.

**Abbreviations:** AuNCs, gold nanocages; DOX, doxorubicin; DOX/AuNCs-PM-HA, DOX-loaded, PM-grafted and HA-modified AuNCs; H22, hepatocarcinoma 22; HA, hyaluronic acid; PM, copolymer of *N*-isopropylacrylamide and acrylamide.

of all mice are shown in Figure 8A, from which we could clearly see that the mice of DOX group significantly lost weight, while the mice of other groups did not. These results indicated that the DOX/AuNCs-PM-HA nanocomplexes did not have systemic toxic side effects, but free DOX did have obvious toxicity. It was also demonstrated that DOX/AuNCs-PM-HA nanocomplexes had good biocompatibility. Generally, the antitumor efficacy could be reflected from the relative tumor volume. As shown in Scheme 1, in contrast to the control, DOX and DOX/AuNCs-PM-HA groups, the mice treated with DOX/AuNCs-PM-HA+NIR had better effect on tumor growth inhibition. It further showed that under NIR irradiation, light could effectively be converted to heat by the AuNCs accumulated at the tumor site, thus stimulating the shrinkage of PM chains to accelerate the release of DOX and produce PPT.

## Histologic analysis

To investigate the influence of DOX/AuNCs-PM-HA on the organs of mice, the mice were sacrificed for further

evaluating the antitumor capability and biotoxicity of NC (control), DOX, DOX/AuNCs-PM-HA and DOX/AuNCs-PM-HA+NIR. The major organs (hearts, livers, spleens, lungs and kidneys) and tumors were collected and stained by H&E. The H&E staining of tumor sections is shown in Figure 8B. From Figure 9, it is clearly shown that the groups of DOX/AuNCs-PM-HA and DOX/AuNCs-PM-HA+NIR had no obvious organ damage; however, the DOX group had severe cardiotoxicity. The heart and spleen of the DOX group had some degree of damage, which conformed with the *in vivo* results of body weight changes and tissue distribution of DOX/AuNCs-PM-HA. In the histology studies, the tumor tissue of the DOX/AuNCs-PM-HA+NIR group showed the highest level of cell damage, revealing a good consistency with the tumor growth data. This further illustrates that the AuNCs-PM-HA could encapsulate DOX very well, and the laser irradiation could stimulate the release of DOX *in vivo*. All the above results indicate that the DOX/AuNCs-PM-HA had high therapeutic effects with good biocompatibility.

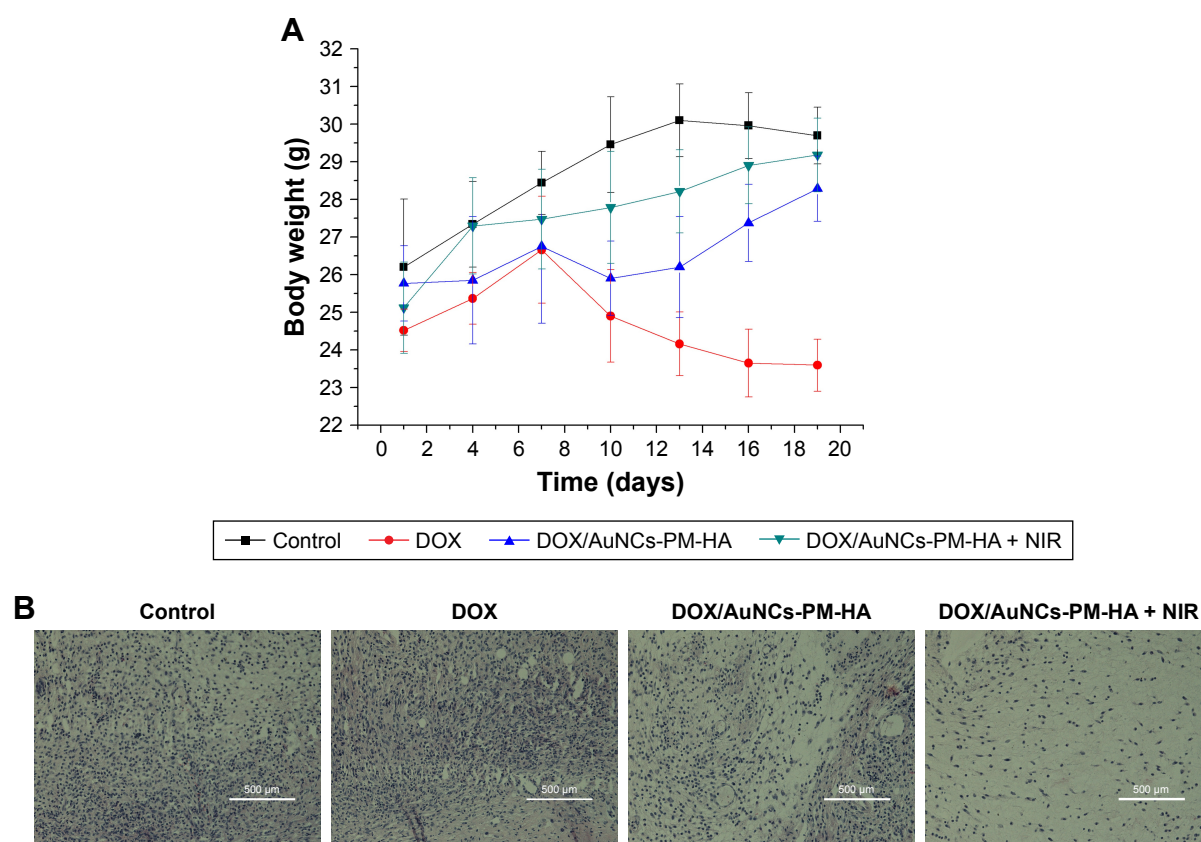


**Figure 8** *In vivo* treatment on H22 tumor-bearing mice with the DOX/AuNCs-PM-HA.

**Notes:** (A) Body weight changes with times of H22 tumor-bearing mice after first treatment with different formulations ( $n=5$ , mean  $\pm$  SD). (B) Hematoxylin and eosin staining of tumor sections collected from different treatment groups (normal saline [control], DOX solution, DOX/AuNCs-PM-HA, DOX/AuNCs-PM-HA+NIR [1.5 W/cm<sup>2</sup>, 808 nm, 7 min] [DOX content at 2 mg/kg]). The scale bars represent 500  $\mu$ m.

**Abbreviations:** AuNCs, gold nanocages; DOX, doxorubicin; DOX/AuNCs-PM-HA, DOX-loaded, PM-grafted and HA-modified AuNCs; DOX/AuNCs-PM-HA+NIR, DOX/AuNCs-PM-HA with NIR laser; H22, hepatocarcinoma 22; HA, hyaluronic acid; NIR, near-infrared irradiation; PM, copolymer of *N*-isopropylacrylamide and acrylamide.

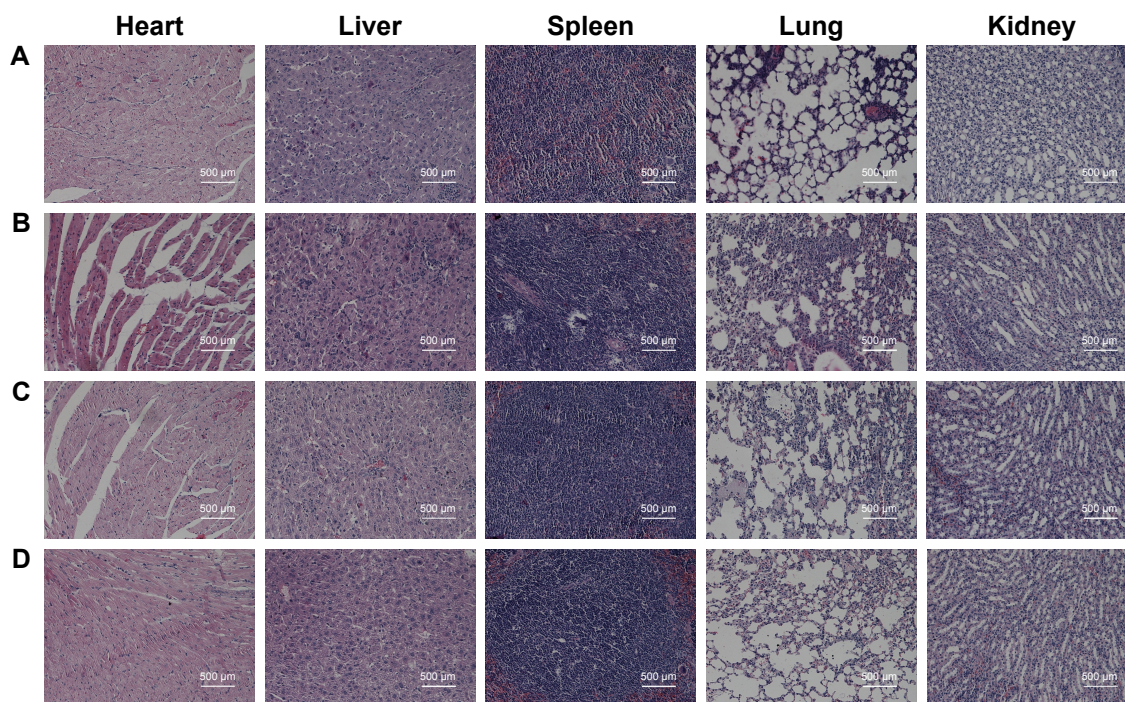


**Figure 9** Histological observation of major organs (hearts, livers, spleens, lungs and kidneys) and tumor sections. The organs were collected from different groups after treatment with different formulations and were stained by H&E.

**Notes:** (A) Normal saline (control), (B) DOX solution, (C) DOX/AuNCs-PM-HA and (D) DOX/AuNCs-PM-HA+NIR (1.5 W/cm<sup>2</sup>, 808 nm, 7 min) (DOX content at 2 mg/kg). The scale bars represent 500 μm.

**Abbreviations:** AuNCs, gold nanocages; DOX, doxorubicin; DOX/AuNCs-PM-HA, DOX-loaded, PM-grafted and HA-modified AuNCs; DOX/AuNCs-PM-HA+NIR, DOX/AuNCs-PM-HA with NIR laser; HA, hyaluronic acid; NIR, near-infrared irradiation; PM, copolymer of *N*-isopropylacrylamide and acrylamide.

## Conclusion

In summary, a novel multi-stimuli-responsive drug delivery system based on DOX/AuNCs-PM-HA core-shell nanocomplexes was developed for the controlled release of anticancer drug and synergistic photothermal-chemotherapy for the first time. The smart gatekeeper, PM shells, would undergo a phase transition along with a change of temperature through the collapse of the polymer chains and reveal the holes of AuNCs to release the packaged DOX. After modification with HA, these nanocomplexes could not only control the drug release with HA degradation by HAase but also target the CD44-positive cancer cells so that they could significantly enhance the therapeutic effect. In vitro studies showed the feasibility of using the DOX/AuNCs-PM-HA nanocomplexes as a drug delivery system. The targeting and biocompatibility of the DOX/AuNCs-PM-HA nanocomplexes were further demonstrated by in vivo studies. What is more, this drug delivery system helped in accurate diagnosis of tumors by PAT imaging and photothermal-chemotherapy. It can be concluded that our DOX/AuNCs-PM-HA system could be used as a promising candidate for the integration of diagnosis and treatment of liver cancer and would provide a new strategy for improved theranostic applications.

## Acknowledgments

This work was financially supported by the National Natural Science Foundation of China (number 81272563) and Key Research Projects of Henan Higher Education Institutions (number 18A350003).

## Disclosure

The authors report no conflicts of interest in this work.

## References

1. Van EM, Murphy BP, Eufrásiodasilva T, et al. Nanomedicines for advanced cancer treatments: transitioning towards responsive systems. *Int J Pharm.* 2016;515(1–2):132–164.
2. Yang Y, Yang Y, Xie X, et al. Dual stimulus of hyperthermia and intracellular redox environment triggered release of siRNA for tumor-specific therapy. *Int J Pharm.* 2016;506(1–2):158–173.
3. Hu X, Wang Y, Zhang L, Man X, Wei D, Zhang J. Redox/pH dual stimuli-responsive degradable Salecan-g-SS-poly(IA-co-HEMA) hydrogel for release of doxorubicin. *Carbohydr Polym.* 2017;155:242–251.
4. Moreira AF, Dias DR, Correia IJ. Stimuli-responsive mesoporous silica nanoparticles for cancer therapy: a review. *Microporous Mesoporous Mater.* 2016;236:141–157.
5. Farzin A, Fathi M, Emadi R. Multifunctional magnetic nanostructured hardystonite scaffold for hyperthermia, drug delivery and tissue engineering applications. *Mater Sci Eng C.* 2016;70:21–31.
6. Liang X, Shang W, Chi C, et al. Dye-conjugated single-walled carbon nanotubes induce photothermal therapy under the guidance of near-infrared imaging. *Cancer Lett.* 2016;383(2):243–249.

7. Liu X, Fang N, Li C, Li X, Liu H, Wu J. A free-standing magneto-fluorescent La 1-x Sr x MnO 3 @ZnO nanoparticle: Synthesis, properties and sharp Curie transition. *J Alloys Compounds*. 2017;693:518–526.
8. Monfared AH, Zamanian A, Beygzadeh M, Sharifi I, Mozafari M. A rapid and efficient thermal decomposition approach for the synthesis of manganese-zinc/oleylamine core/shell ferrite nanoparticles. *J Alloys Compounds*. 2017;693:1090–1095.
9. Huang S, Duan S, Wang J, et al. Folic-Acid-Mediated Functionalized Gold Nanocages for Targeted Delivery of Anti-miR-181b in Combination of Gene Therapy and Photothermal Therapy against Hepatocellular Carcinoma. *Adv Funct Mater*. 2016;26(15):2532–2544.
10. Paliwal SR, Paliwal R, Agrawal GP, Vyas SP. Hyaluronic acid modified pH-sensitive liposomes for targeted intracellular delivery of doxorubicin. *J Liposome Res*. 2016;26(4):276–287.
11. Chen X, Liu Z. A pH-responsive hydrogel based on a tumor-targeting mesoporous silica nanocomposite for sustained cancer labeling and therapy. *Macromol Rapid Commun*. 2016;37(18):1533–1539.
12. Bao S, Huang S, Liu Y, et al. Gold nanocages with dual modality for image-guided therapeutics. *Nanoscale*. 2017;9(21):7284–7296.
13. Ilkhani H, Hughes T, Li J, Zhong CJ, Hepel M. Nanostructured SERS-electrochemical biosensors for testing of anticancer drug interactions with DNA. *Biosens Bioelectron*. 2016;80:257–264.
14. Kurzatkowska K, Santiago T, Hepel M. Plasmonic nanocarrier grid-enhanced Raman sensor for studies of anticancer drug delivery. *Biosens Bioelectron*. 2017;91:780–787.
15. Smith M, Hepel M. Controlled release of targeted anti-leukemia drugs azacitidine and decitabine monitored using surface-enhanced Raman scattering (SERS) spectroscopy. *Mediterranean J Chem*. 2017;6(4):125–132.
16. Leite NT, Hillaireau H, Vergnaud J, et al. Hyaluronic acid-conjugated lipoplexes for targeted delivery of siRNA in a murine metastatic lung cancer model. *Int J Pharm*. 2016;514(1):103–111.
17. Dai L, Zhang Q, Shen X, et al. pH-responsive nanocontainer based on hydrazone-bearing hollow silica nanoparticles for targeting tumor therapy. *J Mater Chem B*. 2016;4:4594–4604.
18. Cai X, Luo Y, Zhang W, Du D, Lin Y. pH-sensitive ZnO quantum dots-doxorubicin nanoparticles for lung cancer targeted drug delivery. *Acs Appl Mater Interfaces*. 2016;8(34):22442–22450.
19. Lin WJ, Lee WC, Shieh MJ. Hyaluronic acid conjugated micelles possessing CD44 targeting potential for gene delivery. *Carbohydr Polym*. 2017;155:101–108.
20. Lin IC, Fang JH, Lin CT, Sung SY, Su YL, Hu SH. Enhanced targeted delivery of cyclodextrin-based supermolecules by core-shell nanocapsules for magnetothermal chemotherapy. *Macromol Biosci*. 2016;16(9):1273–1286.
21. Yang X, Shi L, Guo X, Gao J, Ossipov D. Convergent in situ assembly of injectable lipogel for enzymatically controlled and targeted delivery of hydrophilic molecules. *Carbohydr Polym*. 2016;154:62–69.
22. Danhier F. To exploit the tumor microenvironment: since the EPR effect fails in the clinic, what is the future of nanomedicine? *J Control Release*. 2016;244(Pt A):108–121.
23. Vimala K, Shanthi K, Sundarraj S, Kannan S. Synergistic effect of chemo-photothermal for breast cancer therapy using folic acid (FA) modified zinc oxide nanosheet. *J Colloid Interface Sci*. 2017;488:92–108.
24. Zhang N, Li S, Hua H, et al. Low density lipoprotein receptor targeted doxorubicin/DNA-Gold Nanorods as a chemo- and thermo-dual therapy for prostate cancer. *Int J Pharm*. 2016;513(1–2):376–386.
25. Jin K, Li T, Sánchez-Duffhues G, Zhou F, Zhang L. Involvement of inflammation and its related microRNAs in hepatocellular carcinoma. *Oncotarget*. 2016;8(13):22145–22165.
26. Xu F, Zhang BX, Luo YL. Thermosensitive P(NIPAM-co-AM)-b-PLA block copolymer micelles for applications in intracellular drug delivery. *J Drug Delivery Sci Technol*. 2014;24(2):136–142.
27. Li W, Cai X, Kim C, et al. Gold nanocages covered with thermally-responsive polymers for controlled release by high-intensity focused ultrasound. *Nanoscale*. 2011;3(4):1724–1730.
28. Cambre JN, Roy D, Gondi SR, Sumerlin BS. Facile strategy to well-defined water-soluble boronic acid (co)polymers. *J Am Chem Soc*. 2007;129(34):10348–10349.
29. Scales CW, Convertine AJ, McCormick CL. Fluorescent labeling of RAFT-generated poly(N-isopropylacrylamide) via a facile maleimide-thiol coupling reaction. *Biomacromolecules*. 2006;7(5):1389–1392.
30. De P, Gondi SR, Sumerlin BS. Folate-conjugated thermoresponsive block copolymers: highly efficient conjugation and solution self-assembly. *Biomacromolecules*. 2008;9(3):1064–1070.
31. Gondi SR, And APV, Sumerlin BS. Versatile pathway to functional telechelics via RAFT polymerization and click chemistry. *Macromolecules*. 2007;40(3):474–481.
32. Lima V, Jiang X, Brokken-Zijp J, Schoenmakers PJ, Klumperman B, Linde RVD. Synthesis and characterization of telechelic polymethacrylates via RAFT polymerization. *J Polymer Sci A Polymer Chem*. 2005;43(5):959–973.
33. Zhang Q, Li W, Prof LPW, Dr JC, Prof YX. Facile synthesis of Ag nanocubes of 30 to 70 nm in edge length with CF3COOAg as a precursor. *Chemistry*. 2010;16(33):10234–10239.
34. Skrabalak SE, Au L, Li X, Xia Y. Facile synthesis of Ag nanocubes and Au nanocages. *Nat Protoc*. 2007;2(9):2182–2190.
35. Zhou S, Li J, Gilroy KD, et al. Facile synthesis of silver nanocubes with sharp corners and edges in an aqueous solution. *Acs Nano*. 2016;10(11):9861–9870.
36. Yang J, Shen D, Zhou L, et al. Spatially confined fabrication of core-shell gold nanocages@Mesoporous silica for near-infrared controlled photothermal drug release. *Chem Mater*. 2013;25(15):3030–3037.
37. Li F, Zhao H, Wang ZY, et al. Single palindromic molecular beacon-based amplification for genetic analysis of cancers. *Biosens Bioelectron*. 2017;91:692–698.
38. Zheng T, Li GG, Zhou F, Wu R, Zhu JJ, Wang H. Gold-nanosponge-based multistimuli-responsive drug vehicles for targeted chemophotothermal therapy. *Adv Mater*. 2016;28(37):8218–8226.
39. Mei L, Liu Y, Zhang H, Zhang Z, Gao H, He Q. Antitumor and antimetastasis activities of heparin-based micelle served as both carrier and drug. *Acs Appl Mater Interfaces*. 2016;8(15):9577–9589.
40. He Y, Zhou J, Ma S, et al. Multi-responsive “turn-on” nanocarriers for efficient site-specific gene delivery in vitro and in vivo. *Adv Health Mater*. 2016;5(21):2799–2812.
41. Li Y, Jiang C, Zhang D, et al. Targeted polydopamine nanoparticles enable photoacoustic imaging guided chemo-photothermal synergistic therapy of tumor. *Acta Biomater*. 2017;47:124–134.
42. Li M, Tang Z, Zhang D, et al. Doxorubicin-loaded polysaccharide nanoparticles suppress the growth of murine colorectal carcinoma and inhibit the metastasis of murine mammary carcinoma in rodent models. *Biomaterials*. 2015;51(7):161–172.

## Supplementary materials

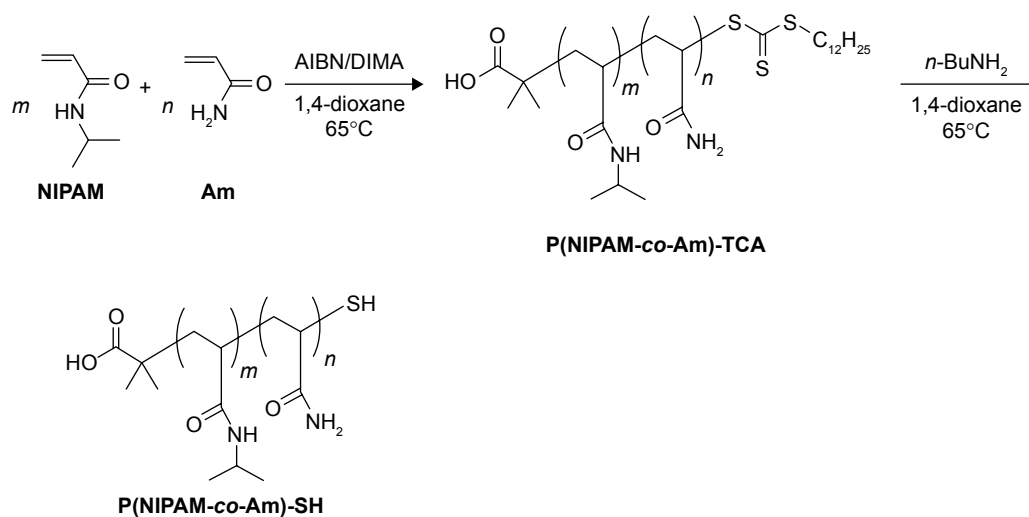


**Figure S1** Synthesis of P(NIPAM-co-Am)-SH copolymers through RAFT copolymerization and end group modification with *n*-butylamine (*n*BuNH<sub>2</sub>).

**Abbreviations:** AIBN, 2,2'-azobis(isobutyronitrile); Am, acrylamide; DIMA, 2-(dodecylthiocarbonothioylthio)-2-methylpropionic acid *N*-hydroxysuccinimide ester; NIPAM, *N*-isopropylacrylamide; RAFT, reversible addition-fragmentation chain transfer; SH, sulfhydryl; TCA, trithiocarbonate.

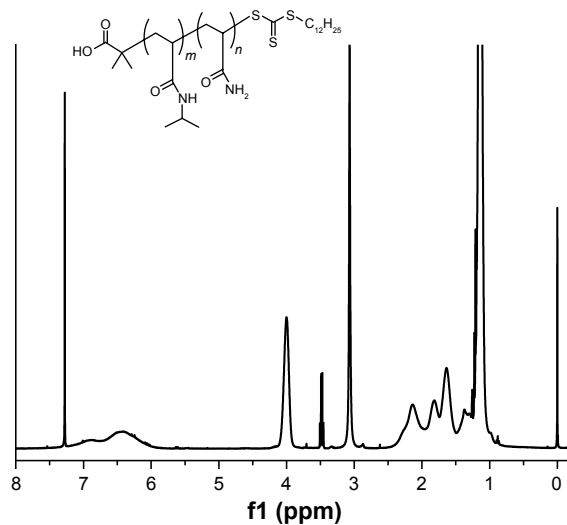


**Figure S2** <sup>1</sup>H-NMR spectrum and structure of P(NIPAM-co-Am) copolymers (in CDCl<sub>3</sub>). 1.02 ppm (d, -CH<sub>2</sub>CH(CH<sub>3</sub>)<sub>2</sub>), 1.16 ppm (s, -NHCH(CH<sub>3</sub>)<sub>2</sub>), 1.30–2.40 ppm (m, polymer backbone protons), 4.03 ppm (s, -NHCH), 4.22 ppm (s, -C(=O)OCH<sub>2</sub>), 6.46 ppm (bs, -C(=O)NH).

**Abbreviations:** Am, acrylamide; bs, broad singlet proton; d, doublet proton; m, multiplet proton; NIPAM, *N*-isopropylacrylamide; NMR, nuclear magnetic resonance; s, singlet proton.

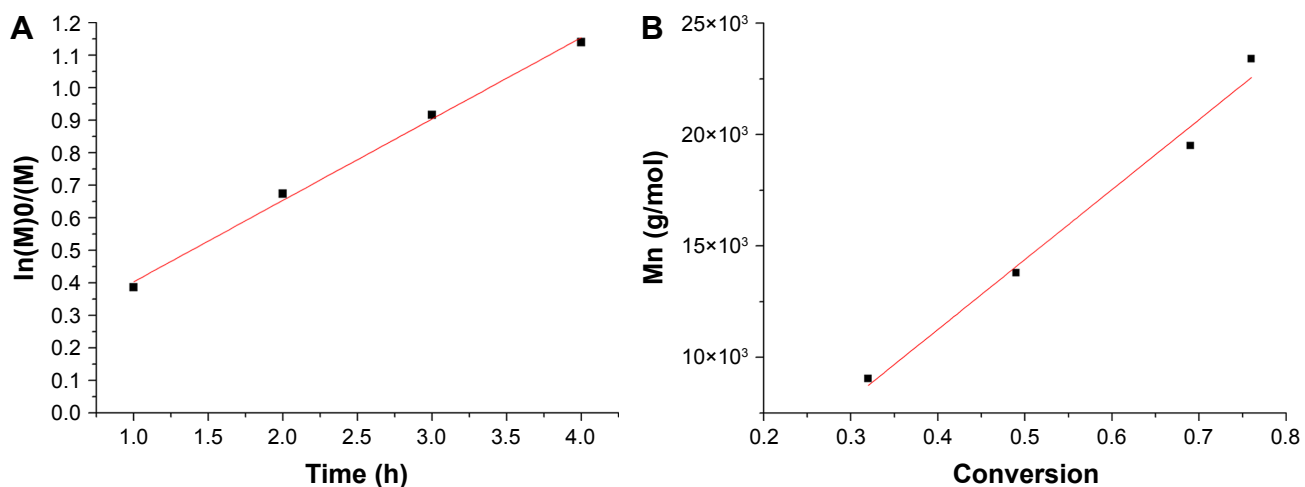


**Figure S3** (A) Kinetic plot of  $\ln(M)_0/(M)$  vs time and (B) the plot of number-average molecular weights ( $M_n$ ) vs monomer conversion for polymerization of NIPAM and Am mediated by DIMA and initiated by AIBN at 65°C in 1,4-dioxane.

**Abbreviations:** AIBN, 2,2'-azobis(isobutyronitrile); Am, acrylamide; DIMA, 2-(dodecylthiocarbonothioylthio)-2-methylpropionic acid *N*-hydroxysuccinimide ester; NIPAM, *N*-isopropylacrylamide.

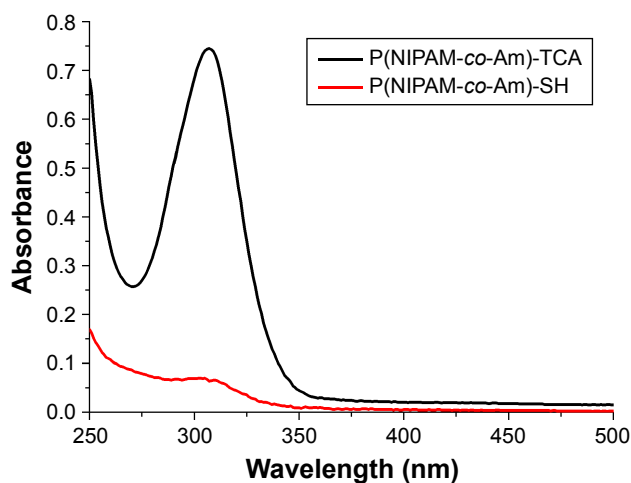


**Figure S4** UV-Vis spectra of poly(NIPAM-co-Am) copolymers (PM, black line) and the aminolysis polymer P(NIPAM-co-Am)-SH (PM-SH, red line) at the concentration of 1 mg/mL in ethanol. The aminolysis of poly(NIPAM-co-Am) copolymer was conducted in the presence of butylamine in 1,4-dioxane at 25°C.

**Abbreviations:** Am, acrylamide; NIPAM, *N*-isopropylacrylamide; PM, copolymer of *N*-isopropylacrylamide and acrylamide; SH, sulfydryl; UV, ultraviolet; Vis, visible.

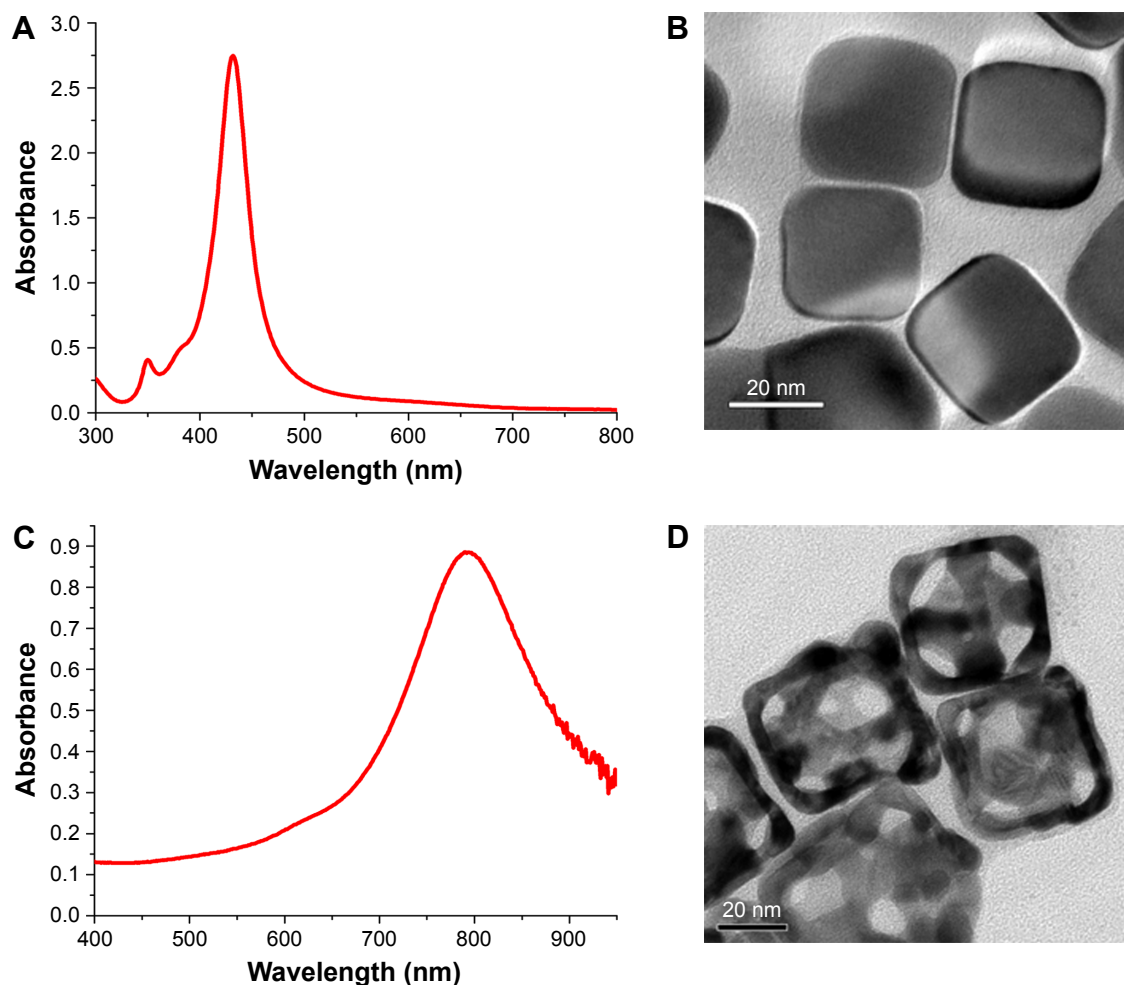


**Figure S5** (A) UV-Vis absorption spectrum and (B) TEM of Ag nanocubes. (C) UV-Vis absorption spectrum and (D) TEM of AuNCs.  
**Abbreviations:** Am, acrylamide; AuNCs, gold nanocages; TEM, transmission electron microscopy; UV, ultraviolet; Vis, visible.

### International Journal of Nanomedicine

#### Publish your work in this journal

The International Journal of Nanomedicine is an international, peer-reviewed journal focusing on the application of nanotechnology in diagnostics, therapeutics, and drug delivery systems throughout the biomedical field. This journal is indexed on PubMed Central, MedLine, CAS, SciSearch®, Current Contents®/Clinical Medicine,

Submit your manuscript here: <http://www.dovepress.com/international-journal-of-nanomedicine-journal>

Journal Citation Reports/Science Edition, EMBase, Scopus and the Elsevier Bibliographic databases. The manuscript management system is completely online and includes a very quick and fair peer-review system, which is all easy to use. Visit <http://www.dovepress.com/testimonials.php> to read real quotes from published authors.

Dovepress